Chaotic mixing in microchannels *via* low frequency switching transverse electroosmotic flow generated on integrated microelectrodes

Hongjun Song,[a] Ziliang Cai,[a] Hongseok (Moses) Noh[b] and Dawn J. Bennett*[a]

Received 3rd September 2009, Accepted 6th November 2009
First published as an Advance Article on the web 5th January 2010
DOI: 10.1039/b918213f

In this paper we present a numerical and experimental investigation of a chaotic mixer in a microchannel *via* low frequency switching transverse electroosmotic flow. By applying a low frequency, square-wave electric field to a pair of parallel electrodes placed at the bottom of the channel, a complex 3D spatial and time-dependence flow was generated to stretch and fold the fluid. This significantly enhanced the mixing effect. The mixing mechanism was first investigated by numerical and experimental analysis. The effects of operational parameters such as flow rate, frequency, and amplitude of the applied voltage have also been investigated. It is found that the best mixing performance is achieved when the frequency is around 1 Hz, and the required mixing length is about 1.5 mm for the case of applied electric potential 5 V peak-to-peak and flow rate 75 μL h^{-1}. The mixing performance was significantly enhanced when the applied electric potential increased or the flow rate of fluids decreased.

Introduction

Micromixing is a critical process in miniaturized analysis systems such as lab-on-a-chip and microfluidic devices.[1–4] However, the mixing of fluids at the microscale faces a big challenge because viscous effects dominate at small scales, where the flow is laminar, and the mixing between different streams in the flow mainly depends on the molecular diffusion. Unfortunately, the diffusive mixing is slow compared with the convective mixing; thus the mixing length for molecular diffusion is always prohibitively long which negates most of the benefits of miniaturization. In recent years, to reduce the mixing length, many efficient chaotic micromixers have been explored. The concept of the chaotic mixer is to generate chaotic advection *via* stretching and folding fluids. Generally, micromixers can be broadly classified as two types: passive micromixers and active micromixers. In passive micromixers, the flow field is perturbed by changing the geometry of channels or adding geometric obstacles. Researchers have developed many passive micromixers focusing on using chaotic advection, such as the square-wave micromixer,[5] the zigzag micromixer,[6] the rapid three-dimensional passive rotation micromixer,[7] the multivortex micromixer,[8] and the staggered herringbone micromixer.[9] In active micromixers, fluids are always perturbed by using an external energy source such as mechanical pulsation,[10,11] acoustic vibration,[12–15] magnetic force,[16] electrohydrodynamic force,[17] electrothermal force,[18] and electroosmotic force.[19–28] Among all these external resources, electroosmotic flow is the most widely used technique for efficient active mixing. One of the common methods is to disturb fluids by generating patterned transverse electroosmotic flow on heterogeneous surface charges with non-uniform, time-independent zeta potentials.[19,20] The heterogeneous surface can be generated by coating the microchannel walls with different materials[19,20] or by applying suitable surface-chemistry treatments.[29,30] An alternative way to change the distribution of the surface charge is to induce a non-uniform zeta potential surface by using a field-effect to mix the fluids.[21,22] However, the fabrication process of the heterogeneous surface was complex. An easier method to enhance the mixing effect is to control the flow pattern by periodically switching the high voltage electric field applied on the different inlets of a T-form channel. Glasgow *et al.*[23] present a design of a microfluidic mixing device in which the electroosmotic flow at the two inlets pulse out of phase to cause the fluid mixing. Lin *et al.*[24] developed an active T-form microfluidic mixer utilizing switching electroosmotic flow operated either in a conventional switching mode or in a pinched switching mode to perform electrokinetically driven mixing. Fu *et al.*[25] also used this scheme to improve the mixing performance by using multiple streams in a microchannel. Although the fabrication of this type of mixer is very simple (only a T-form channel with applied high voltage electric field through the inlets is needed), there are two main disadvantages. At first, the disturbed transverse flow is always quasi two-dimensional (2D), and it is difficult to realize uniform mixing on the cross-section in high depth ratio three-dimensional (3D) channels. In addition, electrodes are always placed at the inlet and outlet in the above devices, so that the electric potential drops along the length of the channel. The required electric voltage is always higher than several hundred volts which require high voltage power supplies. To reduce the required electric potential, integrated microelectrodes are fabricated on the surface of chips, and the distance is on the order of the width of the microchannel. Electroosmotic manipulation with integrated microelectrodes has been applied to mix the fluids under high frequency AC electric fields[26] (AC electroosmotic flow) and DC electric fields.[27,28] However, the

[a]*Department of Mechanical Engineering, University of Maryland Baltimore County, Baltimore, MD, 21250, USA. E-mail: dawnb@umbc.edu*
[b]*Engineering and Mechanics, Drexel University, Philadelphia, PA, 19104, USA*

flow remains a steady helical streamline, and the stretching and folding of fluid remain in the same direction, where the chaotic advection is not very strong.

In this paper, we present a chaotic micromixer *via* periodic switching transverse EOF when a low frequency electric field is applied on a pair of electrodes placed at the bottom of the channel. The flow mechanism is different from AC electroosmotic flow,[26] where the flow is generated by the action of an electric field on its own induced diffuse charge near a polarizable surface such as an electrode plane. In AC electroosmotic flow, the oscillation period of the electric field should be comparable to the charging time, normally several milliseconds. In our design, the oscillation period of the low frequency electric field is much longer than the charging time. Thus, AC electroosmotic flow decays very fast and the flow at each half period can be deemed as DC electroosmotic flow. It is also different from the mixer with a DC electric field,[27,28] where the flow is steady and the stretch and fold of the fluid remain in the same direction. In our design, fluids will be stretched under the transverse electroosmotic flow, and the direction of stretch turns in alternating directions, where the flow is more complex and the chaotic advection is much stronger.

Model and methods

Device fabrication

There are two components of the device: the channel and the patterned microelectrodes. A schematic process is shown in Fig. 1. The channel was fabricated with PDMS by using the soft lithography technique. A cleaned and dried 2.5 inch silicon wafer was used as the substrate. A negative photoresist, SU8-2075, was coated on the wafer with a spin speed of 3000 rpm for 30 s. After the resist had been applied to the substrate, the coated substrate was initially baked on the hot plate for 5 min at 65 °C, and then the temperature was increased to 95 °C for 15 min. The coated substrate was exposed with the mask under UV-light. Following exposure, a post-exposure bake (1 min at 65 °C and 15 min at 95 °C) was performed, and then the photoresist was developed to get the master layer. A curing agent and the PDMS prepolymer (Sylgard184, Dow Corning Company) were mixed in a 1 : 10 weight ratio and allowed to settle for 10 min or longer to remove the air bubbles. The mixture was poured onto the master layer of SU8 on a hot plate for 1 h at 65 °C and into a heat oven at 80 °C overnight. The final channel was obtained by peeling off the PDMS replicas from the master layer. To be able to inject fluid into the microchannel, 1 mm diameter holes were bored at the inlet and outlet positions of the channels. The patterned microelectrodes were fabricated using the standard photolithograph technique. We used gold as the material for the electrodes. To enhance the reliability between gold and the cover glass, a 20 nm thick layer of Ti was first deposited on the cover glass. Following the process, a 50 nm gold layer was deposited over the Ti on the cover glass. To get the electrode pattern, a positive photoresist AZ-P4110 was spun on the top of the gold layer at a speed of 4000 rpm for 30 s. After pre-exposure bake (1 min at 95 °C), the photoresist was exposed under the UV-light using the electrode pattern mask, and was developed for 60 s using the photoresist developer (1 : 4 AZ400K and DI water). Under the protection of the photoresist pattern, Au and Ti can be safely etched by using the etching solution gold etchant (GE-8148) and 2% HF–0.5% HNO_3 solution, respectively, to get the final pattern of microelectrodes. The final device was obtained by aligning and irreversibly bonding the channel layer onto the patterned microelectrodes layer after treating the contact surfaces using the oxygen plasma methodology.

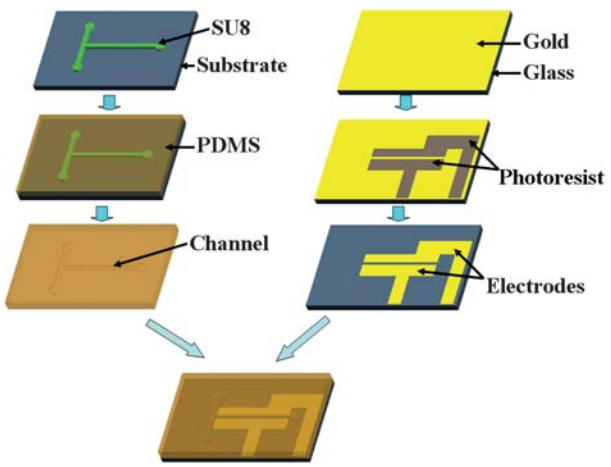

Fig. 1 The fabrication process of the device.

Experimental setup

The sealed chip with electrodes was placed on the object stage. A syringe pump (PHD 2000, Harvard Apparatus, US) was used to drive the prepared solutions. Prior to running the experiments, the channel was cleaned with 0.1 M NaOH solution and rinsed with deionized water to decrease the hydrophobicity of PDMS. Electric fields were generated *via* a synthesized function generator (Protek 9302, Korea) and signals were connected to the electrode pads on the microfluidic chip. A CCD camera attached to the microscope and connected to the computer was used to observe and record the experimental images and videos. To capture the mixing images (in plane or cross-section), a Leica TCS SP5 confocal fluorescence microscopy was used. A 0.1 mM fluorescent dye (Rhodamine B) was dissolved in a 5 mM TES (*N*-[tris-hydroxymethyl]methyl-2-aminoethanesulfonic acid, Sigma). A pure 5 mM TES solution (pH 7.5) was injected into one inlet, and the 5 mM TES solution with Rhodamine B was injected into the other inlet to visualize the mixing process. The cross-sectional images were captured using a 10× air-dry objective lens with the image size 512 × 512 pixels, and the lateral resolution was estimated to be 1 μm.

Numerical method

The governing equations for a viscous incompressible EOF consist of two parts: fluid dynamic equations,

$$\nabla \times V = 0 \tag{1}$$

$$\rho\left(\frac{\partial V}{\partial t} + (V\nabla)V\right) = -\nabla p + \mu\nabla^2 V + \rho_e E \tag{2}$$

and the electrostatic equations

$$E = -\nabla\Phi \tag{3}$$

$$\nabla \times (\sigma \nabla \Phi) = 0 \tag{4}$$

where V is the velocity vector; ρ, p and μ are the density, pressure, and viscosity of the fluid. ρ_e is the charge density; E is the electric field strength; Φ is the electrostatic potential, and σ is the electric conductivity. The mechanical and electrical equations are coupled in terms of the electric field force $\rho_e E$. The velocity should be subjected to the slipless condition on the solid wall $V|_b = 0$. The externally applied electric field is subjected to the insulating boundary conditions on dielectric surfaces $\frac{\partial \Phi}{\partial n}|_b = 0$. The static charge distribution on the solid–liquid interface is simplified and obtained by using the Debye–Hückel approximation:[31]

$$\nabla^2 \varphi = -\rho_e/\varepsilon = \kappa^2 \varphi \tag{5}$$

where $\kappa = \sqrt{\frac{2n_0 e^2 z^2}{\varepsilon k_b T}}$; n_0 is the concentration of the i-th ion at infinity; z_i is chemical valence of the i-th ion; e is the electron charge; k_b is Boltzmann constant; T is the temperature of electrolyte, and ε is the electric permittivity. A well-known Helmholtz–Smoluchowski formulation of the electroosmotic flow velocity is expressed as:

$$U_{EOF} = -\frac{\varepsilon \zeta E}{\mu} \tag{6}$$

here ζ is the surface zeta potential. Eqn (6) shows the electroosmotic flow depends on the applied electric field, the surface zeta potential, the electric permittivity, and the viscosity of the fluid. Increasing the viscosity of the fluid will decrease the electroosmotic flow velocity, where a longer mixing length is required.

The general physical model of this active micromixer is shown in Fig. 2a. A T-type microchannel with two inlets and one outlet is located on the top layer. A pair of parallel patterned electrodes is placed at the bottom of the channel. The length of the channel is 3.5 mm; the width of the channel is 140 μm, and the height of the channel is 60 μm. The width of the electrodes inside the microchannel is about 30 μm, and the distance between the left and right electrodes is 80 μm. As the flow in the microchannel is laminar, and the corresponding Reynolds number is low, the 3D velocity field is approximately decomposed as an axial velocity field u_z and a 2D cavity flow field on the cross-section. The axial velocity is acquired from the Fourier series solution for the rectangular duct flow, and the 2D cavity flow velocity is obtained by solving eqn (1)–(5) for the rectangle geometry of the cross-section with a structured mesh, which contains 280 × 120 grids, by using the commercial software CFD-ACE+ (CFD Research Corporation, Huntsville, AL). To simulate the mixing process, a large number of two different types of particles are injected into the two different inlets. These particles are treated as non-mass and diffusionless (do not affect the flow field). The trajectories of particles in the flow field are obtained by:

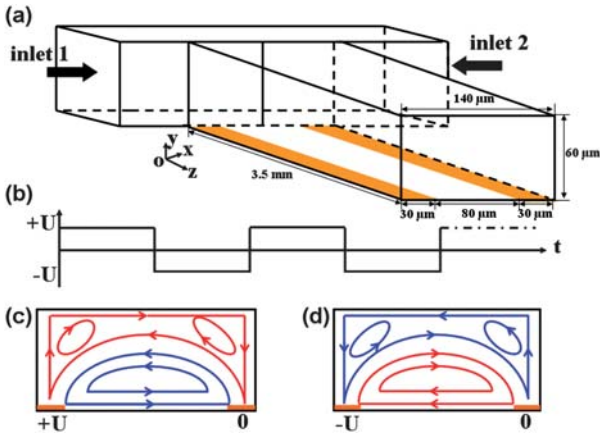

Fig. 2 (a) 3D scheme of the physical model, (b) square-wave electric potential applied on the electrodes, (c) flow diagram of cross-section at the first half period of electric field, and (d) flow diagram of cross-section at the second half period of electric field.

$$\vec{X}(t+\delta t) = \vec{X}(t) + \int_t^{t+\delta t} \vec{u_p}\left(\vec{X}(t), t\right) \mathrm{d}t \tag{7}$$

here $\vec{X}(t)$ is the placement of particle, and $\vec{u_p}(t)$ is the velocity vector of particle at time t. $\vec{X}(t+\delta t)$ is the new position of the particle after one time step δt. The integration process in eqn (7) was performed by a fourth order Runge–Kutta scheme with a constant time step $\delta t = 0.001$ s.

Results and discussion

Mixing mechanism

In our numerical and experimental investigation, a low frequency switching square-wave electric field was applied (shown in Fig. 2b) on the left electrode, and the right electrode was grounded. Due to the non-uniform distribution of the electric field along the walls of channel, there are two recirculations generated. The primary recirculation is generated by the transverse electroosmotic flow near the bottom wall with a higher electric field, and the secondary recirculation is generated by the transverse electroosmotic flow near the side and top wall with a lower electric field. At the first period of electric field, due to the potential of the left electrode being above zero, the transverse electroosmotic flow is generated from the left to the right. Thus, the direction of primary recirculation is counterclockwise and that of the secondary recirculation is clockwise (Fig. 2c). Fluids are stretched and folded under both recirculations. In the second half period, the directions of both recirculations are reversed because the electric potential at the left electrode is below zero (Fig. 2d). Thus, fluids are stretched and folded in the opposite way from the first half period. A three-dimensional (3D) complex spatially and time-dependent flow was generated under these recirculations, whose directions were alternatively changed. Thus fluids were not only stretched but also oscillated on the transverse direction, where chaotic advection was much stronger than that with DC electric field. The uniform mixing generated in 3D channels was different from the quasi 2D mixing process of the active mixers generated by switching the electric field at different inlets 22, 23, 24. To track the mixing profile along the channel, a large number of two types of particles (approximately 14 000 particles for each) were injected into the inlets, and the

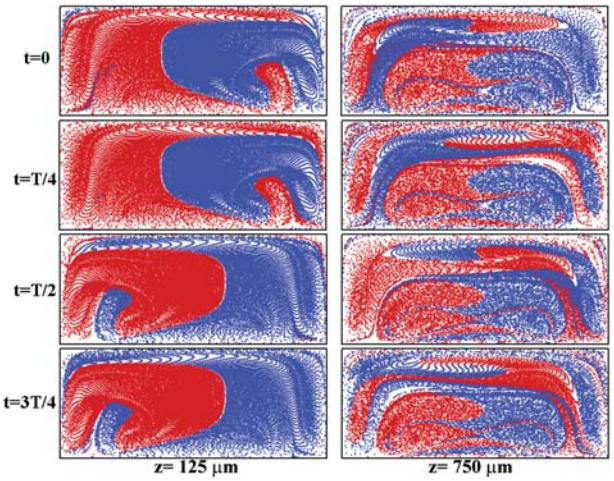

Fig. 3 The mixing images at the cross-section at different times ($t = 0$, $T/4$, $T/2$, $3T/4$) during one period by using the numerical method. Two types of particles were injected into different inlets (denoted as red for particles in the left inlet and blue for the particles in the right inlet) to visualize the mixing process. The left side of the figure shows the mixing images at $z =$ 125 μm, and the right side shows the mixing images at $z = 750$ μm.

distribution of particles on the cross-section at different axial distances was recorded.

Fig. 3 shows the mixing images of these two types of particles along different axial distances $z = 125$ μm and $z = 750$ μm (particles denoted as red color from the left inlet and blue from the right inlet) at different times during one period. The flow rate was 37.5 μL h^{-1}, and applied electric potential was 5 V peak-to-peak at 0.5 Hz. During the first half period, the particles on the left near the bottom were driven from the left to the right and were stretched following the counterclockwise direction due to the primary recirculation, and the particles on the left near the top are stretched following the clockwise direction due to the secondary recirculation. During the second half period, the mixing images were almost symmetric to the images at the first half period because the direction of the recirculations was changed to the opposite way. We found that the mixing images were almost the same during the first half period (images of $t =$ 0 and $t = T/4$ shown in Fig. 3) and the second half period (images of $t = T/2$ and $t = 3T/4$ shown in Fig. 3) at the distance $z =$ 125 μm only the distribution of particles close to the wall were a little different. However, the mixing images become more different during each half period at the distance $z = 750$ μm. This is due to the parabolic distribution of the axial flow under pressure-driven flow. The fluid near the channel wall will require a much longer time to pass the same distance as the fluid near the center of the channel. If the time is larger than half of the period of the electric field, the direction of fluid stretch will change and oscillate in the transverse direction. At $z = 125$ μm, the downstream distance is very short, and the passing time for most of the fluid to reach the cross-section is below half a period of the electric field. Only a little fluid very close to the wall requires a passing time longer than a half period. Most of the fluid remains in the same direction of recirculation, where the image remains almost the same. Only a little fluid very near to the walls oscillates during each half period. When the downstream distance increases to 750 μm ($z = 750$ μm), more of each fluid

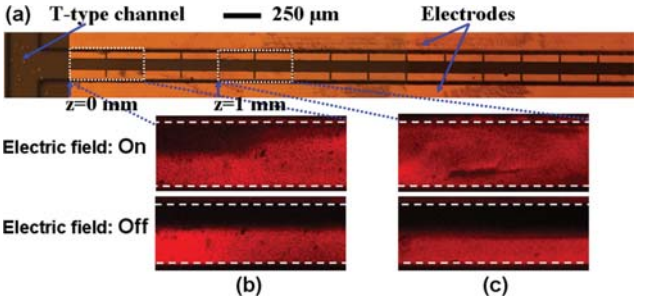

Fig. 4 (a) Microphotograph of the fabricated device, (b) the comparison of confocal fluorescence images of the x–z plane at $y = 30$ μm (half height) at the start point of the electrodes ($z = 0$ mm), and (c) the comparison of the confocal fluorescence images of the x–z plane at $y = 30$ μm (half height) at the downstream distance ($z = 1$ mm). Top figure shows fluids were mixed when the electric field is on and were still separated when the electric field is off. The darker region corresponds to the pure TES solution, and the red color region corresponds to the TES solution with a 0.1 mM a fluorescent dye (Rhodamine B).

moved close to the wall due to the recirculations and required a longer time (bigger than half period of electric field) to pass the same distance than the time if it is kept in the center. More of each fluid was stretched and oscillated with time at the downstream distance $z = 750$ μm during each half period. Thus the mixing images are more complex and change with the time during one period. As the downstream distance increases (the required passing time is longer and more fluid moves near the wall), the movement of the fluids is more intertwined, and the mixing effect is better.

The mixing mechanism was also experimentally investigated. Fig. 4a shows the microphotograph of the fabricated device. Fig. 4b and c show the comparison of confocal fluorescence microscopy images of the x–z plane at $y = 30$ μm (half height) at the starting location of the electrodes ($z = 0$ mm) and at the downstream with a distance 1 mm ($z = 1$ mm), respectively. The applied electric potential is 5 V peak-to-peak at 0.5 Hz, and the flow rate is 37.5 μL h^{-1}. In Fig. 4b, fluids from the two inlets flowed separately when the electric field is off. Only molecular diffusion across the interface can be observed; when the electric field is on, the fluids moved across the interface and mixed due to the transverse electroosmotic flow. In Fig. 4c, most of the two fluids mixed well when the electric field was on and still separated when the electric field was off at $z = 1$ mm.

To further investigate the mixing profile on the cross-section, the mixing images of cross-sections at different downstream distances were also recorded and compared with the numerical results in Fig. 5. The images of the simulation results and the experimental results were shown on the left side and on the right side, respectively. In the numerical simulation, a large number of non-mass and diffusionless particles were injected into the left side, and the distribution of particles were recorded as red color dots in Fig. 5. In the experimental investigation, TES buffer with fluorescent dye (Rhodamine B), which is excited as red color, was injected in the left, and the concentration of fluorescent dye on the cross-sections was also recorded. The flow rate was 37.5 μL h^{-1}, and the applied electric potential was 5 V peak-to-peak at 0.5 Hz for both numerical and experimental investigation. In Fig. 5, the cross-sectional images of the numerical and

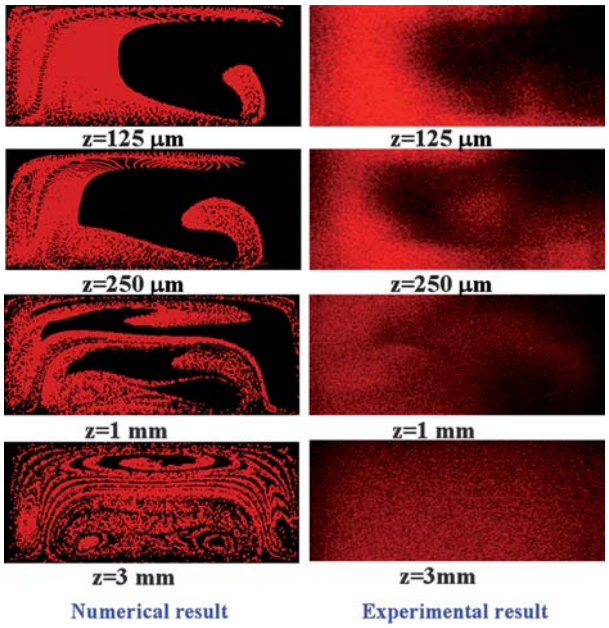

Fig. 5 The comparison of the cross-section images at different downstream distance (z = 125 μm, 250 μm, 1 mm, and 3 mm) between the numerical and experimental results. A large number of particles (denoted as red dot) and TES buffer of 0.1 mM Rhodamine B (denoted as red) were injected into the left inlet in the numerical and experimental investigation, respectively, to visualize the mixing process.

experimental results match well. The fluids started to stretch from the bottom and the top due to the recirculations. The stretch of the fluids was small when the downstream distance was short. It shows that the stretch was increased when the downstream distance increased from 125 μm to 250 μm. When the downstream distance increased to 750 μm, the fluids became more intertwined, and the contact area between two fluids was much larger than in the inlets. We noticed that the numerical results show the particle regions have been split into several strips, but the edge of the strips was dim and difficult to identify in the experimental results. It is reasonable because we assumed the particles were diffusionless in numerical simulations, but the diffusion of fluorescent dye (Rhodamine B) cannot be neglected in the actual experimental investigation. The diffusion coefficient of Rhodamine B is approximate 2×10^{-10} cm^2 s^{-1}, and the corresponding Peclet number is about 1000. We also noticed the stretch shape of the fluids is a little different between the experimental and numerical results. The reason for this discrepancy is because the numerical images were recorded at the exact start of each period, but it was difficult to capture the image at the exact same time in experimental investigation. Nevertheless, the comparison between numerical and experimental results still matches very well. It was clearly shown that particles were split into dozens of thin strips in the numerical simulation at z = 3 mm which indicated that the fluids mixed well. A uniform and completely mixed image was also captured at z = 3 mm in experimental investigation, which matches the numerical images well.

The effects of operational parameters

Further we investigated the effects of operational parameters such as the applied electric frequency, potential, and the flow rate on the mixing performance. The applied electric frequency is the most important parameter and plays a key role for the mixing process. When the frequency increases, the change of recirculation direction is faster, and the flow becomes more time-dependent, which will enhance the mixing effect. However, the mixing performance is also related to the transverse movement of fluids. If the frequency is too high, the oscillation is too fast and fluids cannot travel enough distance to generate valid stretching along the cross-section. Fig. 6 shows the comparison of confocal fluorescence microscopy images of the x–z plane at y = 30 μm (half height) at the starting location of the electrodes (z = 0 mm) and at the downstream with a distance 1 mm (z = 1 mm), respectively, when the electric field frequency varies from 0 Hz to 3 Hz. The applied electric potential is 5 V peak-to-peak, and the flow rate of fluids is 75 μL h^{-1}. It is shown that fluids were strongly stretched on the cross-section when the frequency was under 2 Hz, and fluids oscillated quickly on the transverse direction, and only formed a wave-like structure when the frequency is 2 Hz or higher. Comparing the mixing images at z = 1 mm, we found that the flow is steady when the frequency is zero (DC electric field). Fluid with fluorescent dye moved to the other side along the top and bottom wall due to the recirculations, and the fluid without fluorescent dye moved toward the center (corresponding to a black strip in the center on the image) where the mixing is bad. When the frequency is not zero, the fluids are not only stretched by the recirculations, but also the direction of recirculations will change periodically and generate oscillation on the transverse direction to further enhance the mixing performance. Although part of the fluid in the center mixed well, the oscillation was still slow, and this made it difficult to disturb the other part of the fluid in the center, which formed a small triangular dark zone in the center on the mixing image when the frequency increased to 0.5 Hz. Fig. 6 shows most of the fluid is disturbed by the oscillation and mixed well when the frequency was 1 Hz. However, the mixing performance decreased again when the frequency increased up to 2 Hz and 3 Hz because the

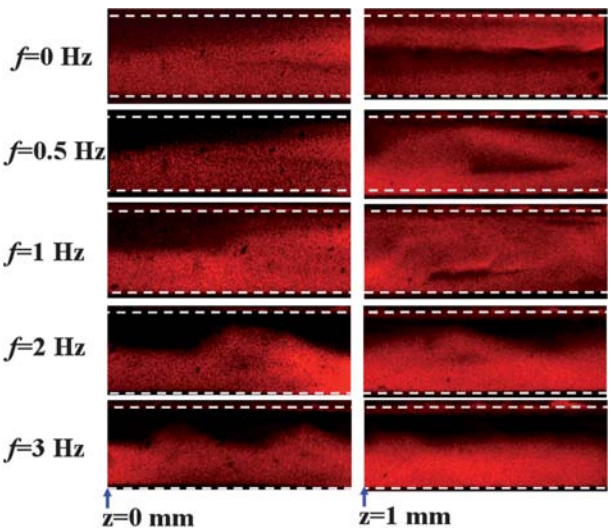

Fig. 6 Fluorescence images of the x–z plane at y = 30 μm (half height) were captured with different electric frequencies (f = 0 Hz, 0.5 Hz, 1 Hz, 2 Hz, and 3 Hz). The left part of the figure shows the images captured at the start point, and the right part of the figure shows the images captured at the downstream (z = 1 mm).

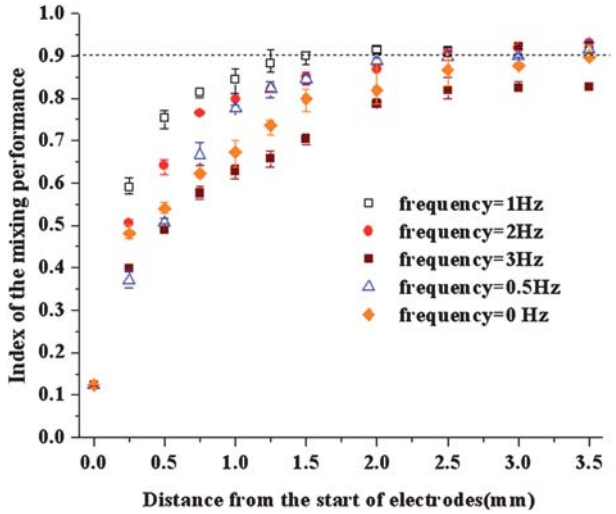

Fig. 7 The index of the mixing performance with different frequencies of the applied electric field. (The applied electric potential is 5 V peak-to-peak, and flow rate is 75 μL h^{-1}).

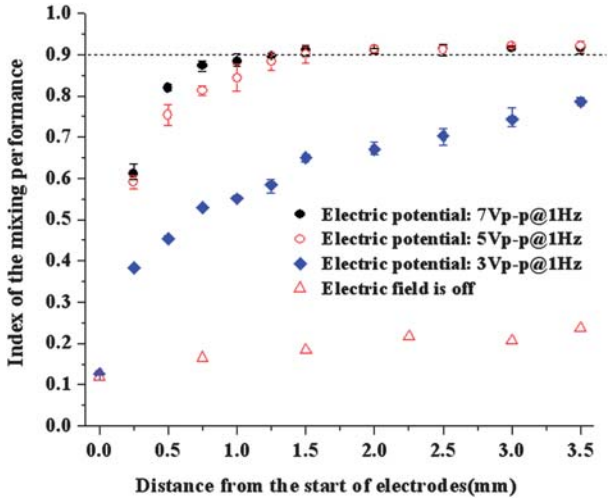

Fig. 8 The index of mixing performance with different applied electric potentials. (The frequency of applied electric field is 1 Hz and flow rate is 75 μL h^{-1}).

flow formed a wave-like pattern due to the oscillation being too fast. The qualitative conclusion from Fig. 6 is that the mixing performance becomes better when the frequency increases from 0 to 1 Hz and decreases when the frequency is increased to 2 Hz or above.

To quantify the mixing performance, we measured the mixing index of the captured cross-section images, which is defined by, $i = 1 - I_s$, where I_s is the discrete intensity of segregation, which is introduced by Danckwert:[32] $I_s = \frac{\left\langle (c - \langle c \rangle)^2 \right\rangle}{\langle c \rangle (c_{max} - \langle c \rangle)}$, where c is the intensity of the pixel; $\langle\ \rangle$ means the average value over all pixels, and c_{max} is the average intensity. In a perfectly mixed system, $I_s = 0$ or the index of mixing performance $i = 1$, while in a completely segregated system, $I_s = 1$ or $i = 0$. Fig. 7 shows the index of mixing performance at different frequencies along with the downstream distance from the start. For each position, the index of mixing performance i was the average value obtained by calculating sequence images with the same time interval and the error bar on the figures shows the deviation range from the average value. We assumed that fluids are completely mixed when the mixing index reaches 0.9 (the dashed line shown in Fig. 7), corresponding to 90% of the fluid being mixed,[9] and the downstream distance is defined as the required mixing length. The shorter the required mixing length, the better is the mixing performance. Fig. 7 shows that fluids were completed mixed when the frequency was below 3 Hz, and only 82% of the fluid was mixed when the frequency was 3 Hz. The corresponding required mixing lengths are approximate 3.5 mm, 2.5 mm, 1.5 mm, and 2.5 mm when the frequency increases from 0 Hz, 0.5 Hz, 1 Hz, and 2 Hz, respectively. This indicates that the mixing performance becomes better when the frequency increased from 0 Hz to 1 Hz and becomes worse when the frequency continuously increases to 3 Hz or higher, which matches the qualitative conclusion based on the analysis of the x–z plane image. The frequency of 1 Hz is the optimal frequency in this case, and the corresponding required mixing length is only 1.5 mm. Fig. 7 also demonstrates that the required mixing length at 1 Hz is much shorter than that by using a DC electric field (frequency = 0 Hz).

The applied electric potential is another important parameter in the mixing process because the strength of the transverse movement is related on the transverse flow velocity, which is linear with the applied electric potential. The comparison of mixing performance with different applied electric potentials is shown in Fig. 8. It shows that only 20% of the fluid is mixed at the outlet when the electric field is off, and 80% of the fluid is mixed at the outlet when the applied electric potential increased to 3 V peak-to-peak. Fluids were completely mixed when the applied electric potential increased to 5 V peak-to-peak and 7 V peak-to-peak with the required mixing lengths of 1.5 mm and 1.25 mm, respectively. This result indicates that the mixing performance was improved rapidly when the applied electric potential

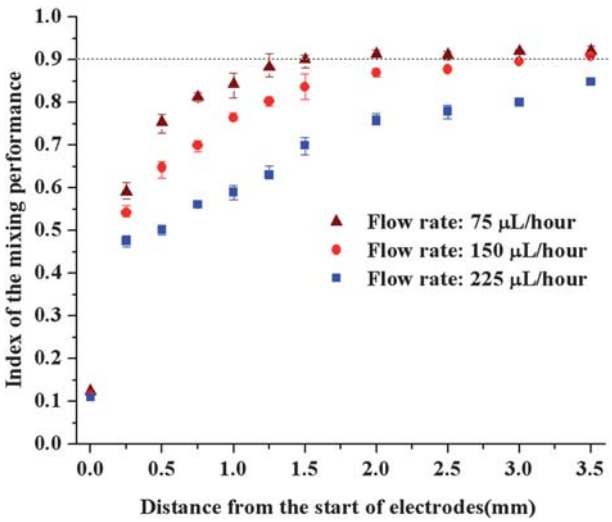

Fig. 9 The index of mixing performance with different flow rates. (The frequency of applied electric field is 1 Hz, and the applied electric potential is 5 V peak-to-peak.)

increased. The required mixing length is relatively short by comparison with the published work.

We should note that the formation of bubbles due to electrolysis is a common problem in electroosmotic flow. We found that a lot of bubbles were generated when applying a DC electric field with the amplitude 3 V. However, the electrolysis is significantly reduced when we apply the low frequency electric field. The mixer worked well and no bubbles were generated when the amplitude of the square-wave electric field increased up to 9 V peak-to-peak.

The flow rate of the fluids is also important for mixing. Increasing the flow rate will reduce the oscillation frequency and increase the Peclet number. The mixing performance becomes worse when the flow rate increases. Fig. 9 shows the comparison of the mixing performance at the flow rates of 75 μL h^{-1}, 150 μL h^{-1}, and 225 μL h^{-1}. Fluid is completely mixed at 1.5 mm when the flow rate is 75 μL h^{-1}. The required mixing length increased to 2.5 mm when the flow rate increased to 150 μL h^{-1}, and only 85% of the fluid was mixed at the outlet when the flow rate increased to 225 μL h^{-1}.

Conclusions

In this paper, we demonstrated a chaotic micromixer to enhance the mixing effect *via* periodical switching transverse EOF, which is generated by applying a low frequency electric field on a pair of electrodes placed at the bottom of the channel. The mixing mechanism was investigated by both numerical and experimental methods. It indicates that a complex 3D spatially and time-dependent flow was generated. Fluids are not only stretched but also oscillate on the transverse direction to significantly enhance the mixing effect. The effects of applied electric frequency, applied electric potential, and flow rate for mixing performance were also discussed. For the case of an applied electric potential of 5 V peak-to-peak and flow rate 75 μL h^{-1}, the mixing performance was improved when we increased the frequency from 0 to 1 Hz, but became worse when the frequency increased to 2 Hz or higher. An optimal frequency of 1 Hz was chosen, and the required mixing length was only 1.5 mm. In addition, the mixing performance was significantly enhanced when the applied electric potential increased from 3 V peak-to-peak to 7 V peak-to-peak, and became worse when the flow rate increased from 75 μL h^{-1} to 225 μL h^{-1}.

Acknowledgements

Hongjun Song thanks Professor Xie-Zhen Yin in the Department of Modern Mechanics at University of Science and Technology of China, Hefei for his guidance and training. The authors thank Chere Petty of Department of Biological Sciences, University of Maryland Baltimore County for her aid in using the Leica SP5 TCS confocal microscope, which is supported by NSF DBI grant no. 0722569.

Notes and references

1 J. M. Ottino and S. Wiggins, *Science*, 2004, **305**, 485–486.
2 H. A. Stone, A. D. Stroock and A. Ajdari, *Annu. Rev. Fluid Mech.*, 2004, **36**, 381–411.
3 C. J. Campbell and B. A. Grzybowski, *Philos. Trans. R. Soc. London, Ser. A*, 2004, **362**, 1069–1086.
4 J. M. Ottino and S. Wiggins, *Philos. Trans. R. Soc. London, Ser. A*, 2004, **362**, 923–935.
5 R. H. Liu, M. A. Stremler, K. V. Sharp, M. G. Olsen, J. G. Santiago, R. J. Adrian, H. Aref and D. J. Beebe, *J. Microelectromech. Syst.*, 2000, **9**, 190–197.
6 V. Mengeaud, J. Josserand and H. Girault, *Anal. Chem.*, 2002, **74**, 4279–4286.
7 S. Park, J. Kim, J. Park, S. Chung, C. Chung and J. K. Chang, *J. Micromech. Microeng.*, 2004, **14**, 6–14.
8 A. P. Sudarsan and V. M. Ugaz, *Proc. Natl. Acad. Sci. U. S. A.*, 2006, **103**, 7228–7233.
9 A. D. Stroock, S. K. Dertinger, A. Ajdari, I. Mezic, H. Stone and G. M. Whitesides, *Science*, 2002, **295**, 647–651.
10 F. Bottausci, I. Mezić, C. D. Meinhart and C. Cardonne, *Philos. Trans. R. Soc. London, Ser. A*, 2004, **362**, 1001–1018.
11 X. Niu, L. Liu, W. Wen and P. Sheng, *Appl. Phys. Lett.*, 2006, **88**, 153508–153511.
12 Z. Yang, H. Goto, M. Matsumoto and R. Maeda, *Electrophoresis*, 2000, **21**, 116–119.
13 Z. Yang, S. Matsumoto, H. Goto, M. Matsumoto and R. Maeda, *Sens. Actuators, A*, 2001, **93**, 266–272.
14 W. K. Tseng, J. L. Lin, W. C. Sung, S. H. Chen and G. B. Lee, *J. Micromech. Microeng.*, 2006, **16**, 539–548.
15 T. Frommelt, M. Kostur, M. Wenzel-Schäfer, P. Talkner, P. Hänggi and A. Wixforth, *Phys. Rev. Lett.*, 2008, **100**, 0345021–0345024.
16 G. Mensing, T. Pearce, M. Graham and D. Beebe, *Philos. Trans. R. Soc. London, Ser. A*, 2004, **362**, 1059–1068.
17 O. El Moctar, N. Aubry and J. Batton, Electro-hydrodynamic micro-fluidic mixer, *Lab Chip*, 2003, **3**, 273–280.
18 M. Sigurdson, D. Z. Wang and C. D. Meinhart, *Lab Chip*, 2005, **5**, 1366–1373.
19 E. Biddiss, D. Erickson and D. Li, *Anal. Chem.*, 2004, **76**, 3208–3213.
20 K. Fushinobu and M. Nakata, *Trans. ASME J. Electronic Packaging*, 2005, **127**, 141.
21 H. Y. Wu and C. H. Liu, *Sens. Actuators, A*, 2005, **118**, 107–115.
22 J. L. Lin, K. H. Lee and G. B. Lee, *Electrophoresis*, 2005, **26**, 4605–4615.
23 I. Glasgow, J. Batton and N. Aubry, *Lab Chip*, 2004, **4**, 558–562.
24 C. H. Lin, L. M. Fu and Y. S. Chien, *Anal. Chem.*, 2004, **76**, 5265–5272.
25 L. M. Fu, R. J. Yang, C. H. Lin and Y. S. Chien, *Electrophoresis*, 2005, **26**, 1814–1824.
26 N. Sasaki, T. Kitamori and H. B. Kim, *Lab Chip*, 2006, **6**, 550–558.
27 H. J. Song, X. Z. Yin and D. Bennett, *ASME International Mechanical Engineering Congress and Exposition*, ASME, Chicago, US, 2006.
28 N. Lynn, C. Henry and D. Dandy, *Microfluid. Nanofluid.*, 2008, **5**, 493–505.
29 W. L. W. Hau, D. W. Trau, N. J. Sucher, M. Wong and Y. Zohar, *J. Micromech. Microeng.*, 2003, **13**, 272–278.
30 S. Krishnamoorthy, J. Feng, A. Henry, L. Locascio, J. Hickman and S. Sundaram, *Microfluid. Nanofluid.*, 2006, **2**, 345–355.
31 P. Debye and E. Hückel, *Z. Phys.*, 1923, **24**, 85–206.
32 P. V. Danckwerts, *Appl. Sci. Res.*, 1952, **3**, 279–296.

